Channel water storage anomalies: A new remotely sensed measurement for global river analysis

Stephen Coss[1,2*] , Michael T Durand[1,2] , C.K. Shum[1,2] , Yuchan Yi[1], Xiao Yang[3], Tamlin Pavelsky[3], Augusto Getirana[4,5], Dai Yamazaki[6]

[1]Ohio State University, Columbus, OH
[2]Byrd Polar and Climate Research Center, Columbus, OH
[3]University of North Carolina at Chapel Hill, Chapel Hill, NC
[4] Hydrological Sciences Laboratory, NASA Goddard Space Flight Center, Greenbelt, MD
[5]Science Applications International Corporation, Greenbelt, MD, United States
[6]Institute of Industrial Science, The University of Tokyo, Meguro-ku, Tokyo, Japan

Corresponding author: Stephen Coss (coss.31@osu.edu)

Key Points:

- We introduce a 26-year record of entirely remotely sensed volumetric channel water storage anomaly.
- Storage climatology amplitude represents (0.05-13.8%) terrestrial water storage variability but just just 0.2% of basin area.
- This new measurement can be used to analize river spatial storage paderns in a way that was previously unprecedented.

Abstract

River channels store large volumes of water globally, critically impacting ecological and biogeochemical processes. Despite the importance of river channel storage, there is not yet an observational constraint on this quantity. We introduce a 26-year record of entirely remotely sensed volumetric channel water storage anomaly (VCWS) on 26 major world rivers. We find mainstem VCWS climatology amplitude (VCWSCA) represents an appreciable amount of basin-wide terrestrial water storage variability (median 2.2%, range 0.05-13.8% across world rivers), despite the fact that mainstem rivers themselves represent an average of just 0.2% of basin area. We find that two global river routing schemes coupled with land surface models reasonably approximate VCWSCA (within ±50%) in only 19.2 % and 23.1 % of rivers considered (by model). These findings demonstrate VCWS is a useful measurement for assessing global hydrological model performance, and for advancing understanding of spatial patterns in global hydrology.

Plain Language Summary

Rivers are a critical part of global hydrology, but until now the variation in how much water rivers store has not been observed directly on the global scale. We created a 25 year recored of this measurement across 26 of the worlds largest rivers. We found that the storage variation in river main channels can represent up to 13% of the total water variation in a river basin despite only representing 0.2% of the total surface area. We also find that current methods to estimate this quantity through modeling (global river routing schemes coupled with land surface models) are only representing this quantity within 50% of the measured value on between 19.2% to 23.1% of the rivers we studied. This demonstrates that this new measurement has value in assessing model proformance and advancing the way we think about how rivers function as water storage vessals.

1 Introduction

While spaceborne sensors have revolutionized our understanding of global hydrology, some terms in the global water cycle remain poorly observed (Lettenmaier et al., 2015). For example, while the Gravity Recovery And Climate Experiment (GRACE; Tapley et al., 2004, 2019) and GRACE Follow-On satellite missions have provided invaluable measurements of global water storage variability (Rodell et al., 2018), they measure the total terrestrial water storage (TWS) anomaly, but do not provide information on the dynamics of individual TWS components such as soil moisture, snow, ground and surface water.

Surface water storage (SWS) in natural and artificial reservoirs, floodplains, wetlands and river channels is critical to human society and ecosystems, but a complete picture of surface water storage dynamics from remote sensing measurements has remained elusive (Döll et al., 2012; Oki & Kanae, 2006). Getirana et al. (2017) modeled SWS globally (neglecting anthropogenic impacts) and estimated that on average, SWS contributes just 8% of overall TWS variability; it is thus difficult to estimate SWS by difference, i.e. by subtracting estimates of other storage terms from GRACE TWS measurements (e.g., Llovel et al., 2010; Swenson et al., 2008; Syed et al., 2008). Remote sensing measurements have shed light on storage change in major world floodplains (Papa et al., 2013; 2015), and on storage in global lakes and reservoirs (Gao et al., 2012; Tortini et al., 2020). However, an observation-based quantification of storage change in rivers has been lacking.

A comprehensive dataset of observations of volumetric changes of water in rivers has not been previously presented, despite the potential value of such observations and the relative simplicity with which such variations can be measured. Time-varying river storage changes

would have value in understanding global water balance and within-watershed variations in TWS. Kim et al. (2009) demonstrated that rivers are major contributors (between 0 and 70%) to TWS variation by modeling river (channel and sub-surface), snow and soil moisture contributions to TWS; however, their work did not separate surface water from underground flow. As noted above, Getirana et al. (2017) found that in most basins the SWS:TWS variability ratio was low, but its maximum value (27%) for the Amazon basin indicated that, for some regions, surface water can play a major role in storage dynamics. We hypothesize that rivers are frequently hotspots of water storage variability, a part of watersheds where much greater water storage change tends to occur than elsewhere. E.g., major rivers typically exhibit seasonal water level measuring several meters, while GRACE TWS seasonal changes are usually < 100 mm across the entire basin. The global measurements of river storage presented in this paper let us quantify these dynamics and help validate model estimates of rivers, which increasingly simulate global river processes (Emery et al., 2018; Getirana, Kumar, et al., 2017; Yamazaki et al., 2011). Finally, storage variations of water in rivers is crucial for ecological and biogeochemical processes. Indeed, storage variations are driven by the same basic hydrologic quantities that drive hyporheic exchange: variations in river depth and surface area. Because water surface elevations (Calmant et al., 2008; Coss et al., 2020; Tourian et al., 2016) and river surface water extent (Allen & Pavelsky, 2018; Huang et al., 2012; Yamazaki et al., 2015) datasets exist, long-term storage variations in rivers can be measured directly, by simply combining water surface elevation (WSE) and width observations, both of which are measured entirely from satellite platforms.

Here, we present the first published data product of volumetric river channel water storage anomaly (VCWS) over 26 of the world's largest rivers using remotely sensed river WSEs and widths in the Global River Radar Altimetry Time Series 1 Kilometer Daily (GRRATS1kd, Coss et al., 2019a). In the context of VCWS we define "anomaly" as the difference between a value at a particular time, and some reference time, t (e.g. the first date in our dataset). Storage change is the time derivative of storage, and can be calculated from the time derivative of the storage anomaly. GRACE TWS is also either a storage anomaly or storage change measurement; in this paper we use "TWS" to refer to storage anomaly. We use the new GRRATS1kd dataset to address three questions: How large are storage variations within river mainstems compared to basin storage variations measured by GRACE? What controls spatial patterns of storage variations in rivers? How do measured river storage variations compare to modeled values?

2 Methods and Datasets

GRRATS1kd is a one kilometer-one day resolution interpolated dataset spanning 26 of the world's largest rivers (Coss et al., 2019a); a list of the rivers is given in Table 1. GRRATS1kd comprises satellite altimetry measurements of river WSE interpolated to 1 km daily resolution, and VCWS estimates computed from interpolated WSE and width. The virtual station data GRRATS (Coss et al., 2019b), is further described in (Coss et al., 2020). In this section, we briefly describe the datasets and major steps used to compute VCWS.

The primary input datasets used to create GRRATS1kd are measurements of river WSE at the intersection of radar altimeter ground tracks and rivers, known as virtual stations (VS) (GRRATS, described by (Coss et al., 2020)), and river width measurements obtained using

RivWidthCloud, a Landsat processing algorithm for measuring river width based on Google Earth Engine (Yang et al., 2019).We use a total of 914 GRRATS VSs spanning 1992-2018 leveraging seven altimeters (ERS-1, TOPEX/Poseidon, ERS-2, JASON-1, Envisat, OSTM/Jason-2, Jason-3). (https://doi.org/10.5067/PSGRA-SA2V1). Note that Coss et al. (2020) describes version 1 of GRRATS, which included only 2 altimeters. The VSs processed by Coss et al. (2020) included all locations on ocean-draining main-stem rivers with a mean width of 900m or greater. The 26 rivers used for this study are those with enough data density to interpolate a daily 1km resolution WSE (26 of 39). RivWidthCloud was used to process a total of 53,924 Landsat images in order to generate a total of 115.2 million (2.2 million after 1km averaging and quality filtering) channel width measurements.

In GRRATS1kd, VCWS is computed as follows. First, we statistically reprocess the GRRATS VS data to remove outliers using a moving window *t*-test (Coss et al., 2020). Second, we interpolate VS WSEs to 1 km daily resolution, by grouping VS data by altimeter constellation, bilinear interpolation of anomaly on a flow distance-time grid, smoothing, adding back a digital elevation model (DEM) value to convert back to absolute WSE (DEM selection is identical to the description in Coss et al., (2020)), and finally forcing WSEs to decrease downriver at each time step. Third, for each 1 km location downstream, we create a piecewise-linear relationship between WSE and width (W) as described in the supplemental material (S1). These piecewise linear relationships between W and WSE can be represented as: $= f_x(WSE)$.

VCWS in units of km^3 can be calculated by integrating the W-WSE relationships at location x:

$$VCWS_{x,t} = \Delta_x \int_{WSE_{x,t1}}^{WSE_{x,t}} f_x(WSE) dWSE, \quad (1)$$

where the x subscript indicates that these values (as well as the piecewise linear relationships between WSE and W) are specific to one 1 km segment, and Δ_x is the segment resolution, and t_1 is the initial time in the series (typically a date in April 1992). Thus, VCWS has dimensions of cubic volume, and can be thought of as the product of river cross-sectional area anomaly (the integral term in Eq. 1, units of m^2) and Δ_x. When we present timeseries of river total VCWS values, we simply sum $VCWS_{x,t}$ over all spatial locations x(Figure 1A). Note that reservoirs are flagged and removed.

For model comparisons (described below)), we analyzed data from two global SWS datasets. Both the Hydrological Modeling and Analysis Platform (Getirana et al., 2012; Getirana, Peters-Lidard, et al., 2017) and the Catchment-based Macro-scale Floodplain model (Yamazaki et al., 2011; 2014) are river routing schemes capable of simulating river and floodplain dynamics. They are forced with surface runoff and baseflow simulated by land surface models. For the data we analyzed, temporal resolution is daily, spatial resolution is1° (~100 km) for HyMAP and 0.1 ° (~10 km) for CaMa-Flood, and the temporal domain is 2002-2017 for HyMAP and 2000-2011 for CaMa-Flood.

Below, we present three separate analyses of climatologies constructed from our data. First we compare with GRACE long-term average TWS climatology. The GRACE data presented is from the Center for Space Research at the University of Texas at Austin (http://www2.csr.utexas.edu/grace). The Data are monthly Mascon solutions spanning 2002-2018, with a 0.25 degree resolution, with an 11 month gap from July of 2017- May of 2018 between GRACE missions (Hosseini-Moghari et al., 2020; Save et al., 2016). For each basin, we

create a 26 year VCWS climatology (VCWSC) summed over the length of the river (Figure 2B). We then measure the amplitude of VCWSC (VCWSCA). Some analyses below present VCWSCA normalized by basin drainage area (i.e. we divide the VCWSC amplitude value by the basin drainage area); we refer to this quantity as channel water storage (CWS) following the definition for GRACE TWS, CWS is presented with units of mm, and is comparable to GRACE. Figure 1 for example, shows the Mississippi VCWSCA is 7.12 km^3 while the drainage are is 3,244,506 km^2. Dividing VCWSCA by drainage area results in a CWS of ~2.2mm. Basin areas are from the United Nations Chief Executive Officer Water Mandate (2016) and World Bank Major River Basins (2017)datasets.

In our discussion of the relationship of CWS to GRACE we reference mean slope data from (Coss et al., 2019b, 2020) and calculate an aridity index from net radiation from Clouds and the Earth's Radiant Energy System (CERES; Loeb et al., 2018; Wielicki et al., 1996) and Global Precipitation Climatology Project (GPCP; Adler et al., 2003).

Second, we relate VCWSCA, mean river width, and basin area at 1km resolution and test if different basin area groups have different CWSA/width relationships. To compare VCWSCA regimes, we relate our VCWSCA data to basin drainage area from Frasson et al., (2019). We first distinguished groups by large increases in flow accumulation to avoid comparison across large tributaries. We then re-assimilate any divisions that did not achieve a change in basin drainage area>10%. Finally, we plot VCWSCA and mean width by 1 km section and perform a simple least squares liner regression on each group. To verify that their slopes are appreciably different, we use the Z test outlined in Paternoster et al.,(1998), with a threshold of 2 for failing the null hypotheses (slopes are the same). Third, we compare with global models by scaling the

GRRATS1kd data up to the model grid resolution (1 or 0.1 degrees), by summing all of our 1 km VCWS data points that fall within each model grid cell. We then examine two criteria: 1) The VCWSCA for all cells overlapping measured channel; 2) Correlation coefficient of each model cell, with the average measured VCWSCA from those measured sections that fell within the cell.

3 Results and Discussion

3.1 The magnitude of main stem CWS as it relates to GRACE TWS

CWS ranges from 0.02 mm to 21.9 mm (on the Zambezi and Ayeyarwada rivers, respectively), with a mean value of 5.36 mm (Figure 2). As expected, the largest values are primarily from tropical basins. Table 1 shows the ratio of CWS compared with GRACE TWS (CWS:TWS ratio hereafter) climatology data constructed from Save et al. (2016) for each of the study river basins Note that for GRACE comparison the Ganges and Brahmaputra basins have been combined. CWS:TWS ratio ranges from 0.05% to 13.8% (on the Zambezi and Uruguay Rivers respectively), with an average of 3.5 % of GRACE TWS being measured in river main stems. That the main stem river contribute an average of several percent of all basin storage variability is perhaps surprising when considering that mainstem rivers constitute on average just 0.2% of total basin area (Table 1). This analysis highlights rivers as storage hotspots, parts of major drainage basins where an oversized fraction of storage variation takes place.

CWS:TWS varies over two orders of magnitude on study rivers, evincing tremendous diversity across global basins in rivers' role in overall basin storage. As the mainstem combines both upstream hydrologic processes and river hydraulics, we explored the role of basin aridity index (AI, defined as the ratio of long-term average potential evaporation to precipitation; see (McMahon et al., 2013) and mainstem slope in the CWS:TWS. We hypothesized that basins with

high AI would have a lower total runoff, and thus a lower CWS:TWS ratio, and that basins with low slope would likely have slower flow velocities, longer channel residence times, and thus larger CWS:TWS ratios. Note AI is presented for only 18 of the 25 basins due to data availability. Overall, we found that these hypotheses bear out in generally, but a predictive relationship was not identified. Specifically, we found that all three rivers with a CWS:TWS ratio above 5.5% were both low slope (<2727 cm/km) and low AI (<0.88). Similarly, 6 of the 8 rivers with a CWS:TWS ratio below 2% had a relatively high AI (>1). Neither slope nor AI correlated linearly with the CWS :TWS ratio, however. For example, the Tocantins and St Lawrence rivers have low AI (< 1), but still have a but still have a low CWS:TWS ratio (approximately 1%). We speculate that other factors such as spatiotemporal variability of precipitation patterns and snow storage also play a role; the Congo, for instance has a two peak hydrograph due to its position under the inter-tropical convergence zone (e.g., Alsdorf et al., 2016)), limiting the predictive power of the AI on basin hydrology (e.g. McMahon et al., 2013).). The human influence due to dams, and storage of water in large floodplains likely also play a role. As a final effort to understand CWS:TWS ratio, we hypothesized simply that basins with larger proportion of their surface area represented by the mainstem would similarly also have a larger CWS:TWS ratio. A linear relationship was identified between these quantities (see Table 1), with $R^2 = 0.54$ and $p = 0$, but this is in part due to the Uruguay river, which can be considered an outlier, with CWS :TWS of nearly 14%. Excluding the Uruguay, $R^2 = 0.1717$ and $p = 0.042$. This result means that the correlation between measured area and CWS:TWS ratio is only significant, when the Uruguay is included. In summary, rivers are storage hotspots within major drainage basins, manifesting orders of magnitude larger storage variability than on average. There is significant variability

among river basins in how large a role the mainstem plays in basinwide storage dynamics, however, it is unclear what factors drive this variability.

3.2 VCWSCA Regimes

While we might expect VCWSCA to increase monotonically with distance downstream, this is frequently not the case. As we can see from the Congo (Figure 2) we sometimes see the opposite, and most frequently find that VCWSCA hotspots occur in a variety of locations on the mainstem of a river (Amazon, Mississippi). Controls on spatial patterns of VCWSCA in rivers are diverse and complex. The Amazon, for example, has large flood plain lakes that suppress surface elevation variation (Bonnet et al., 2008). In an effort to quantify this phenomenon, we compare the relationship between VCWSCA and mean channel width, and basin drainage area at 1 km resolution for 19 of the rivers for which drainage area data are available from Frasson et al. (2019). Generally, as width increases, the VCWSCA increases as well (Figure 4). This is not a uniformly applicable principle, however. Relative Amplitude (e.g. Figure 1a) does not increase uniformly in all rivers as they widen downstream. This means consideration of variation in space is critical for understanding individual rivers' VCWS signature. However, some rivers further show distinct relationships that can be explained by drainage area. Because of the river sections being analyzed, only 15 of the 19 rivers can be subdivided into 2 or more distinguishable (drainage area difference > 10%) groups. For these 15 rivers, we are able to isolate two distinct patterns in the relationship between VCWSCA, mean width, and drainage area. For the first pattern (exemplified by Figure 4a), the slope of the VCWSCA: width relationship does not change with drainage area; for the second pattern (e.g. Figure 4b), the slope changes significantly. We find that 9 rivers show significant changes their VCWSCA: width

relationship with variation in drainage area (Table 1). While the basins with changing slope are broadly geographically distributed, all but one of the non-changing slope basins (Columbia) are near-equatorial (within 30°N of the equator). One possible explanation for this result is that as noted above, large floodplain lakes and floodplain-mainstem interaction in many equatorial basins control water level variation so dramatically, that changes in drainage area downstream produce no distinct change in the spatial patterns of storage variations.

3.3 Model Comparisons

While comparison of GRRATS1kd with HyMAP and CaMa-flood reveals promising similarity between model and measured data on some rivers (Figure 3), HyMAP and CaMa-flood reasonably approximate VCWSCA in 23.1% and 19.2% of the rivers respectively. We define "reasonable" as having a climatology amplitude within ±50% (Wrzesien et al., 2017). We show the cumulative distribution function of these amplitude comparisons for all rivers in Figure 3D (amplitude ratios<4) to provide a more comprehensive view of these data. With few exceptions, the model and measurements are generally in phase; Figure 3c is an exception. To assess the capabilities of the models to represent spatial patterns in VCWSCA, we also compared the Spatial Normalized VCWSCA, that is the spatial series of measured and modeled VCWSCA, after gridding GRRATS1kd onto the model grid. In general, we found that the models represent the seasonal amplitude better than spatial patterns. At the grid cell level, we compared seasonal amplitude from the models and our measurements. For CaMa-flood we find that 50% of rivers (26.9% that were statistically significant) have an average cell correlation >0 (12% >0.5), with a maximum value of 0.8. HyMAP results show 62% of rivers (12.5% that were statistically significant) with an average cell correlation >0 (15% >0.5), with a maximum value of

0.9. Overall these results demonstrate that while models often represent the magnitude of this signal well, they tend to misrepresent the location of the water. Variation in scaling and model precipitation inputs could be responsible for many of the differences we see between the models and measured values. In some extreme cases, we looked at the VCWS components (width and height variation) from the model in greater depth and found that the standard deviation of height is often much higher than measured. It is possible that overestimation of height variation and simplified width variation heavily impact where this variation happens in the models.

5 Conclusions

Here we use a new remote sensing dataset (VCWS) to explore the role of major world rivers in the global water cycle. We find that rivers are storage hotspots, parts of major drainage basins where an exceptionally large fraction of total storage variation takes place. Specifically, by comparing our dataset with GRACE, we showed that the mainstem river accounted for a highly variable percentage (0.05%-13.8%) of all water storage changes within the basin, among the drainage basins analyzed. We hypothesize that a complex array of factors, including basin hydrology and river hydraulics, govern the ratio of river to total water storage change among basins; our preliminary results show that basic factors such as basin-averaged aridity index and river slope do not explain these variations.

We find that within-river spatial patterns in channel water storage climatology anomaly are highly complex, and do not simply increase monotonically with distance downstream as we hypothesized they would. Frequently the opposite pattern emerges, though highly variable hotspot patterns are most common. We find that while the width and channel water storage

climatology relationship generally changes with flow accumulation (expected behavior), this is not always the case (40% do not). The expected behavior generally occurs in near equatorial basins, highlighting that complex hydraulics (tributary backwater, ice jams etc.) might be a much more significant cause of storage variation in rivers at higher latitudes. Third, we find global river routing schemes tend to capture the amplitude of river storage variations more successfully than they represent the spatial nature of how rivers store their water. We find that models represent channel water storage climatology anomaly reasonably (±50%) in only 19.2% and 23.1% of rivers considered (by model). We also find that model cells significantly correlate spatially with measured data on just 26% and 12.5% of rivers (by model). We did not diagnose the cause of these discrepancies, but hypothesize that effects of anthropogenic management (not simulated by the models) play an important role. Future work should explore assimilation of channel water storage into such models, as well as integration with existing datasets measuring floodplains and reservoirs. Such work is even more important, given recent and future datasets that represent improved height and inundated area measurements from sensors such as Planet, Sentinel -2, Landsat 8+9 and the upcoming SWOT mission (Boshuizen et al., 2014; Drusch et al., 2012; Fu et al., 2009; MarkhamM et al., 2019; Roy et al., 2014).

Acknowledgments and Data

The authors report no conflicts of interest.
The data used in this study (DOI: 10.5067/PSGRA-DA2V2) is available on the NASA PO.DAAC (https://podaac.jpl.nasa.gov/dataset/PRESWOT_HYDRO_GRRATS_L2_DAILY_VIRTUAL_STATION_HEIGHTS_V2?ids=&values=).

This work was supported by a NASA FINESST award (GRT00054946).

References

Allen, G. H., & Pavelsky, T. M. (2018). Global extent of rivers and streams. *Science*, *361*(6402), 585. https://doi.org/10.1126/science.aat0636

Alsdorf, D., Beighley, E., Laraque, A., Lee, H., Tshimanga, R., O'Loughlin, F., et al. (2016). Opportunities for hydrologic research in the Congo Basin. *Reviews of Geophysics*, *54*(2), 378–409. https://doi.org/10.1002/2016RG000517

Bonnet, M. P., Barroux, G., Martinez, J. M., Seyler, F., Moreira-Turcq, P., Cochonneau, G., et al. (2008). Floodplain hydrology in an Amazon floodplain lake (Lago Grande de Curuaí). *Journal of Hydrology*, *349*(1), 18–30. https://doi.org/10.1016/j.jhydrol.2007.10.055

Boshuizen, C., Mason, J., Klupar, P., & Spanhake, S. (2014). Results from the planet labs flock constellation.

Calmant, S., Seyler, F., & Cretaux, J. F. (2008). Monitoring continental surface waters by satellite altimetry. *Surveys in Geophysics*, *29*(4–5), 247–269.

CEO Water Mandate. (2016). Retrieved April 22, 2020, from http://ceowatermandate.org/riverbasins.

Coss, S., Durand, M., Lettenmaier, D., Yi, Y., Jia, Y., Guo, Q., et al. (2019a). Pre SWOT Hydrology GRRATS Daily River Heights and Storage Version 2. *PO.DAAC*. https://doi.org/10.5067/PSGRA-DA2V2

Coss, S., Durand, M., Lettenmaier, D., Yi, Y., Jia, Y., Guo, Q., et al. (2019b). Pre SWOT Hydrology GRRATS Virtual Station River Heights Version 2. NASA Physical Oceanography DAAC. https://doi.org/10.5067/PSGRA-SA2V2

Coss, S., Durand, M., Yi, Y., Jia, Y., Guo, Q., Tuozzolo, S., et al. (2020). Global River Radar Altimetry Time Series (GRRATS): new river elevation earth science data records for the

hydrologic community. *Earth Syst. Sci. Data*, *12*(1), 137–150. https://doi.org/10.5194/essd-12-137-2020

Döll, P., Hoffmann-Dobrev, H., Portmann, F. T., Siebert, S., Eicker, A., Rodell, M., et al. (2012). Impact of water withdrawals from groundwater and surface water on continental water storage variations. *Journal of Geodynamics*, *59–60*, 143–156. https://doi.org/10.1016/j.jog.2011.05.001

Drusch, M., Del Bello, U., Carlier, S., Colin, O., Fernandez, V., Gascon, F., et al. (2012). Sentinel-2: ESA's optical high-resolution mission for GMES operational services. *Remote Sensing of Environment*, *120*, 25–36.

Emery, C. M., Paris, A., Biancamaria, S., Boone, A., Calmant, S., Garambois, P.-A., & da Silva, J. S. (2018). Large-scale hydrological model river storage and discharge correction using a satellite altimetry-based discharge product. *Hydrology and Earth System Sciences*, *22*(4), 2135.

Frasson, R. P. de M., Pavelsky, T. M., Fonstad, M. A., Durand, M. T., Allen, G. H., Schumann, G., et al. (2019). Global relationships between river width, slope, catchment area, meander wavelength, sinuosity, and discharge. *Geophysical Research Letters*, *46*(6), 3252–3262.

Fu, L.-L., Alsdorf, D., Rodriguez, E., Morrow, R., Mognard, N., Lambin, J., et al. (2009). The SWOT (Surface Water and Ocean Topography) mission: spaceborne radar interferometry for oceanographic and hydrological applications. Presented at the OCEANOBS'09 Conference, Citeseer.

Gao, H., Birkett, C., & Lettenmaier, D. P. (2012). Global monitoring of large reservoir storage from satellite remote sensing. *Water Resources Research*, *48*(9). https://doi.org/10.1029/2012WR012063

Getirana, A., Boone, A., Yamazaki, D., Decharme, B., Papa, F., & Mognard, N. (2012). The hydrological modeling and analysis platform (HyMAP): Evaluation in the Amazon basin. *Journal of Hydrometeorology*, *13*(6), 1641–1665.

Getirana, A., Kumar, S., Girotto, M., & Rodell, M. (2017). Rivers and Floodplains as Key Components of Global Terrestrial Water Storage Variability. *Geophysical Research Letters*, *44*(20), 10,359-10,368. https://doi.org/10.1002/2017GL074684

Getirana, A., Peters-Lidard, C., Rodell, M., & Bates, P. D. (2017). Trade-off between cost and accuracy in large-scale surface water dynamic modeling. *Water Resources Research*, *53*(6), 4942–4955. https://doi.org/10.1002/2017WR020519

Hosseini-Moghari, S.-M., Araghinejad, S., Ebrahimi, K., Tang, Q., & AghaKouchak, A. (2020). Using GRACE satellite observations for separating meteorological variability from anthropogenic impacts on water availability. *Scientific Reports*, *10*(1), 15098. https://doi.org/10.1038/s41598-020-71837-7

Huang, S., Li, J., & Xu, M. (2012). Water surface variations monitoring and flood hazard analysis in Dongting Lake area using long-term Terra/MODIS data time series. *Natural Hazards*, *62*(1), 93–100. https://doi.org/10.1007/s11069-011-9921-6

Kim, H., Yeh, P. J., Oki, T., & Kanae, S. (2009). Role of rivers in the seasonal variations of terrestrial water storage over global basins. *Geophysical Research Letters*, *36*(17).

Lettenmaier, D. P., Alsdorf, D., Dozier, J., Huffman, G. J., Pan, M., & Wood, E. F. (2015). Inroads of remote sensing into hydrologic science during the WRR era. *Water Resources Research*, *51*(9), 7309–7342.

Llovel, W., Becker, M., Cazenave, A., Crétaux, J.-F., & Ramillien, G. (2010). Global land water storage change from GRACE over 2002–2009; Inference on sea level. *Comptes Rendus Geoscience*, *342*(3), 179–188.

Loeb, N. G., Su, W., Doelling, D. R., Wong, T., Minnis, P., Thomas, S., & Miller, W. F. (2018). 5.03 - Earth's Top-of-Atmosphere Radiation Budget. In S. Liang (Ed.), *Comprehensive Remote Sensing* (pp. 67–84). Oxford: Elsevier. https://doi.org/10.1016/B978-0-12-409548-9.10367-7

Major River Basins Of The World. (2017, July 24). Retrieved January 1, 2018, from https://datacatalog.worldbank.org/dataset/major-river-basins-world

MarkhamM, B., Barsi, J., Donley, E., Efremova, B., Hair, J., Jenstrom, D., et al. (2019). Landsat 9: Mission status and prelaunch instrument performance characterization and calibration (pp. 5788–5791). Presented at the IGARSS 2019-2019 IEEE International Geoscience and Remote Sensing Symposium, IEEE.

McMahon, T., Laaha, G., Parajka, J., Peel, M., Savenije, H., Sivapalan, M., et al. (2013). Prediction of annual runoff in ungauged basins.

Oki, T., & Kanae, S. (2006). Global hydrological cycles and world water resources. *Science*, *313*(5790), 1068–1072.

Papa, F., Frappart, F., Güntner, A., Prigent, C., Aires, F., Getirana, A. C. V., & Maurer, R. (2013). Surface freshwater storage and variability in the Amazon basin from multi-

satellite observations, 1993–2007. *Journal of Geophysical Research: Atmospheres*, *118*(21), 11,951-11,965. https://doi.org/10.1002/2013JD020500

Papa, F., Frappart, F., Malbeteau, Y., Shamsudduha, M., Vuruputur, V., Sekhar, M., et al. (2015). Satellite-derived surface and sub-surface water storage in the Ganges–Brahmaputra River Basin. *Groundwater Systems of the Indian Sub-Continent*, *4*, 15–35. https://doi.org/10.1016/j.ejrh.2015.03.004

Paternoster, R., Brame, R., Mazerolle, P., & Piquero, A. (1998). Using the correct statistical test for the equality of regression coefficients. *Criminology*, *36*(4), 859–866.

Rodell, M., Famiglietti, J. S., Wiese, D. N., Reager, J. T., Beaudoing, H. K., Landerer, F. W., & Lo, M.-H. (2018). Emerging trends in global freshwater availability. *Nature*, *557*(7707), 651–659. https://doi.org/10.1038/s41586-018-0123-1

Roy, D. P., Wulder, M. A., Loveland, T. R., Woodcock, C., Allen, R. G., Anderson, M. C., et al. (2014). Landsat-8: Science and product vision for terrestrial global change research. *Remote Sensing of Environment*, *145*, 154–172.

Save, H., Bettadpur, S., & Tapley, B. D. (2016). High-resolution CSR GRACE RL05 mascons. *Journal of Geophysical Research: Solid Earth*, *121*(10), 7547–7569.

Swenson, S., Famiglietti, J., Basara, J., & Wahr, J. (2008). Estimating profile soil moisture and groundwater variations using GRACE and Oklahoma Mesonet soil moisture data. *Water Resources Research*, *44*(1).

Syed, T. H., Famiglietti, J. S., Rodell, M., Chen, J., & Wilson, C. R. (2008). Analysis of terrestrial water storage changes from GRACE and GLDAS. *Water Resources Research*, *44*(2).

Tapley, B. D., Bettadpur, S., Watkins, M., & Reigber, C. (2004). The gravity recovery and climate experiment: Mission overview and early results. *Geophysical Research Letters*, *31*(9).

Tapley, B. D., Watkins, M. M., Flechtner, F., Reigber, C., Bettadpur, S., Rodell, M., et al. (2019). Contributions of GRACE to understanding climate change. *Nature Climate Change*, *9*(5), 358–369.

Tortini, R., Noujdina, N., Yeo, S., Ricko, M., Birkett, C. M., Khandelwal, A., et al. (2020). Satellite-based remote sensing data set of global surface water storage change from 1992 to 2018. *Earth System Science Data*, *12*(2), 1141–1151. https://doi.org/10.5194/essd-12-1141-2020

Tourian, M., Tarpanelli, A., Elmi, O., Qin, T., Brocca, L., Moramarco, T., & Sneeuw, N. (2016). Spatiotemporal densification of river water level time series by multimission satellite altimetry. *Water Resources Research*.

Wielicki, B. A., Barkstrom, B. R., Harrison, E. F., Lee, R. B., III, Smith, G. L., & Cooper, J. E. (1996). Clouds and the Earth's Radiant Energy System (CERES): An Earth Observing System Experiment. *Bulletin of the American Meteorological Society*, *77*(5), 853–868. https://doi.org/10.1175/1520-0477(1996)077<0853:CATERE>2.0.CO;2

Wrzesien, M. L., Durand, M. T., Pavelsky, T. M., Howat, I. M., Margulis, S. A., & Huning, L. S. (2017). Comparison of methods to estimate snow water equivalent at the mountain range scale: a case study of the California Sierra Nevada. *Journal of Hydrometeorology*, *18*(4), 1101–1119.

Yamazaki, D., Kanae, S., Kim, H., & Oki, T. (2011). A physically based description of floodplain inundation dynamics in a global river routing model. *Water Resources Research*, *47*(4). https://doi.org/10.1029/2010WR009726

Yamazaki, D., Sato, T., Kanae, S., Hirabayashi, Y., & Bates, P. D. (2014). Regional flood dynamics in a bifurcating mega delta simulated in a global river model. *Geophysical Research Letters*, *41*(9), 3127–3135. https://doi.org/10.1002/2014GL059744

Yamazaki, D., Trigg, M. A., & Ikeshima, D. (2015). Development of a global ~ 90 m water body map using multi-temporal Landsat images. *Remote Sensing of Environment*, *171*, 337–351. https://doi.org/10.1016/j.rse.2015.10.014

Yang, X., T. M. Pavelsky, G. H. Allen, & G. Donchyts. (2019). RivWidthCloud: An Automated Google Earth Engine Algorithm for River Width Extraction From Remotely Sensed Imagery. *IEEE Geoscience and Remote Sensing Letters*, 1–5. https://doi.org/10.1109/LGRS.2019.2920225

Figure 1.

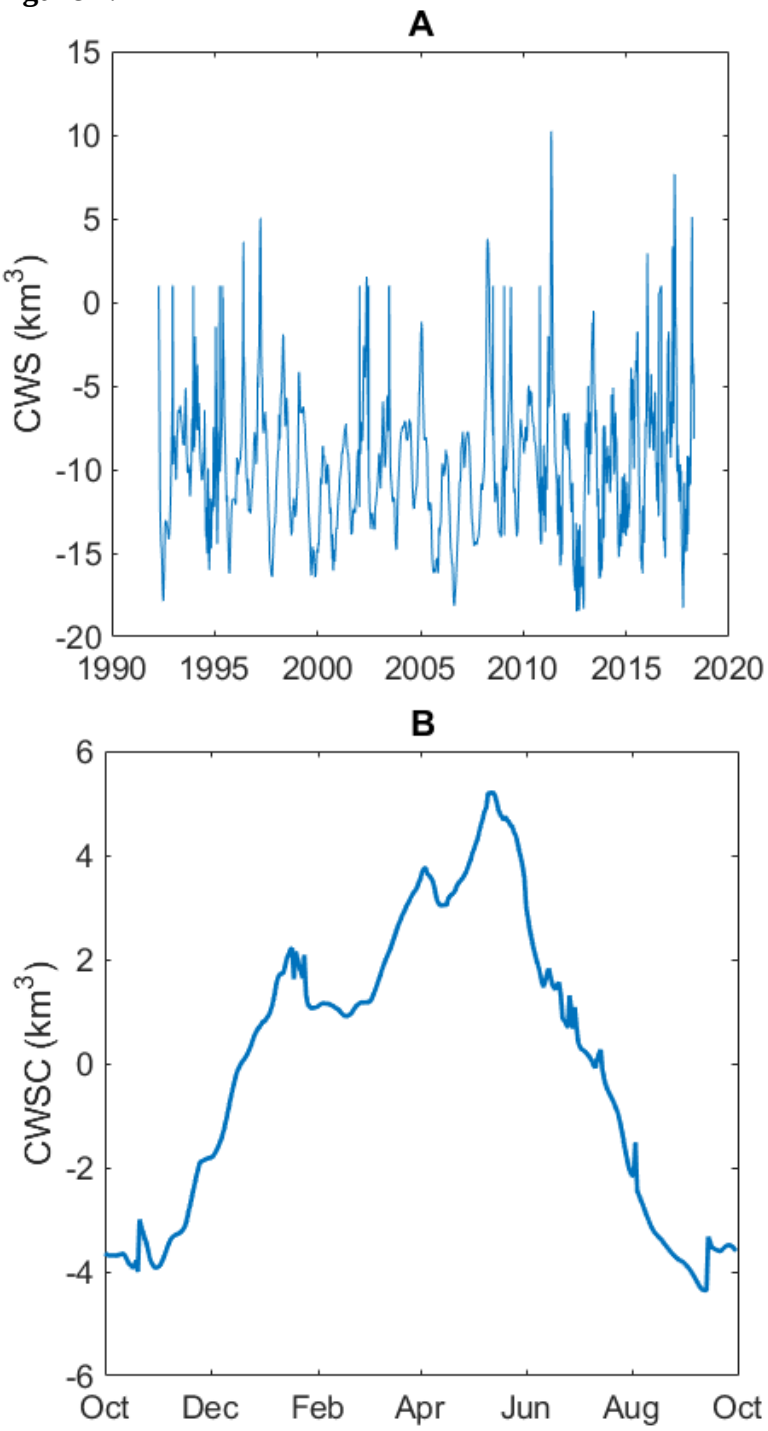

Figure 1. Mississippi VCWS time series. Panel A is the complete record, while panel B shows constructed climatology (VCWSC). The Mississippi climatology amplitude (VCWSCA) is 7.1245 km^3 while the drainage area is 3,244,506 km^2. Dividing VCWSCA by drainage area results in a CWS of ~2.2mm.

Figure 2.

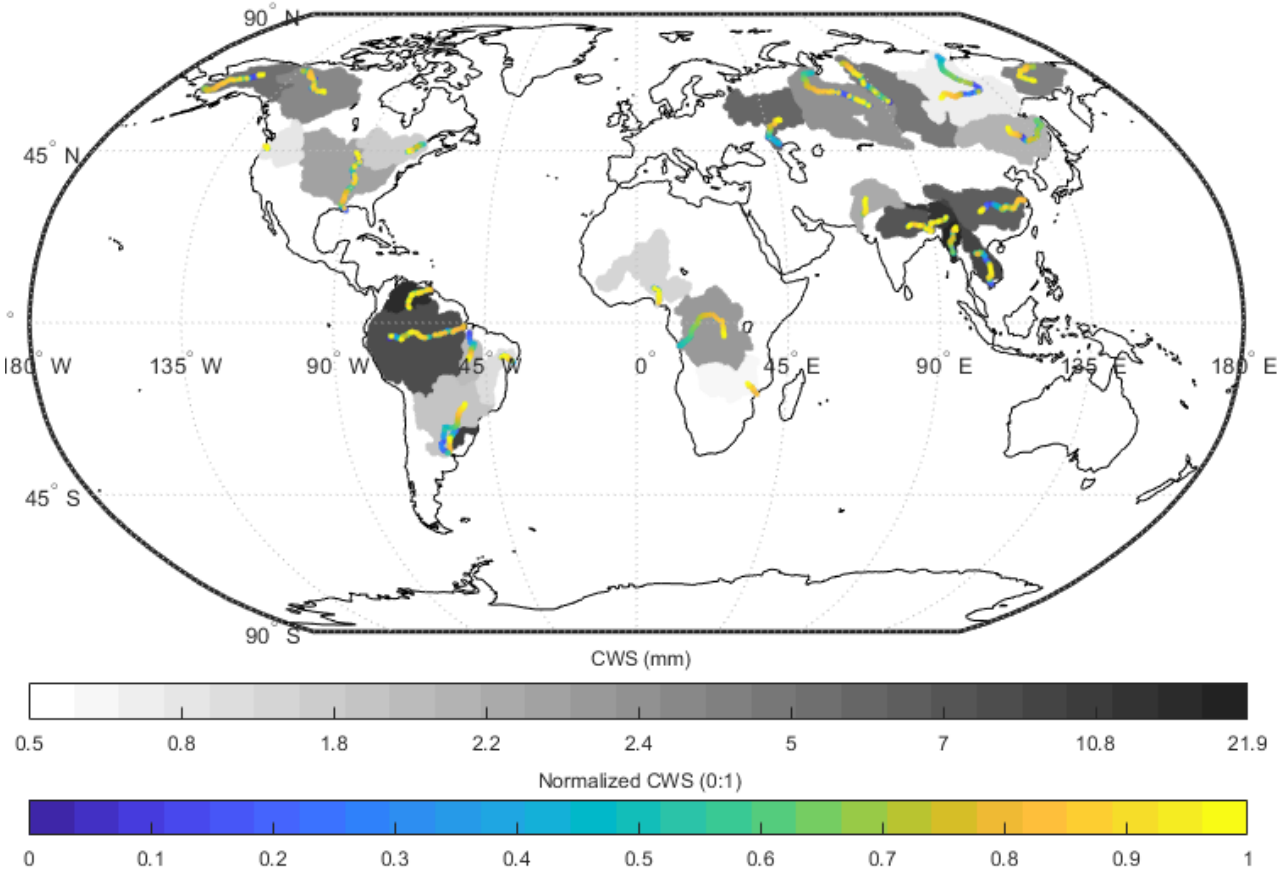

Figure 2. CWS (basin normalized VCWSCA in mm) shown in greyscale. Individual 1km VCWSCA segment data shown in blue-yellow color scale rescaled between zero and 1 (following formula S1) to highlight where rivers store their water. Every 100th point shown.

Figure 3.

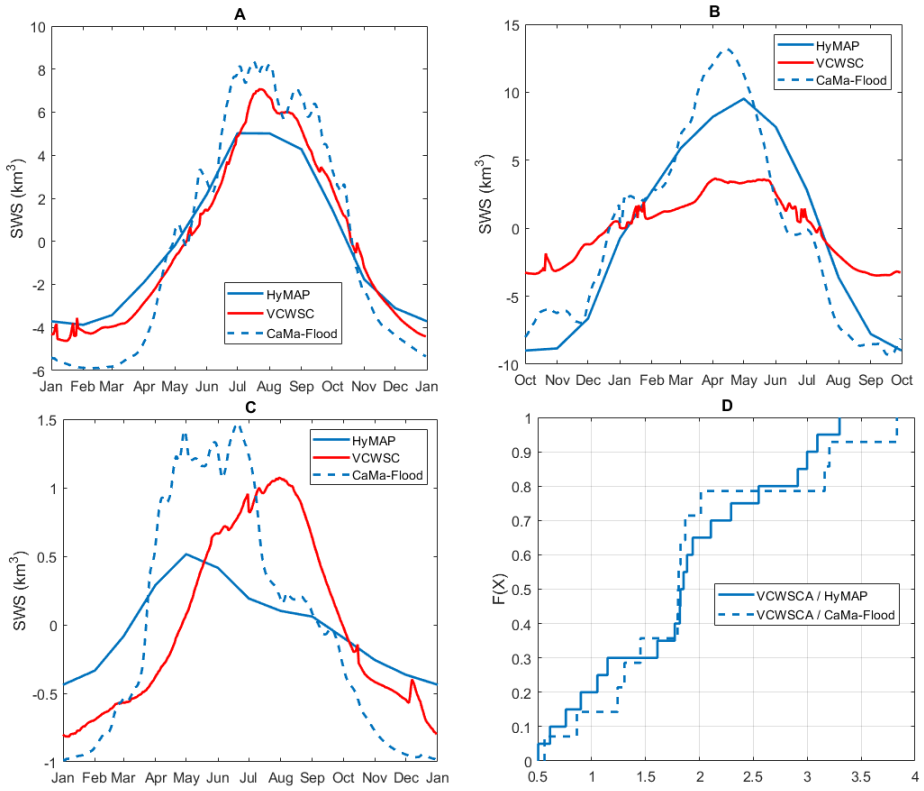

Figure 3 Storage change climatology plots for the Brahmaputra (A), Mississippi (B), and Indus (C) Rivers. HyMAP data is shown in solid blue, CaMa-flood is shown in dashed blue, and Measured VCWSCA is shown in red panel D shows the CDF of amplitude ratio comparisons from both models (amplitude ratios<4).

Figure 4.

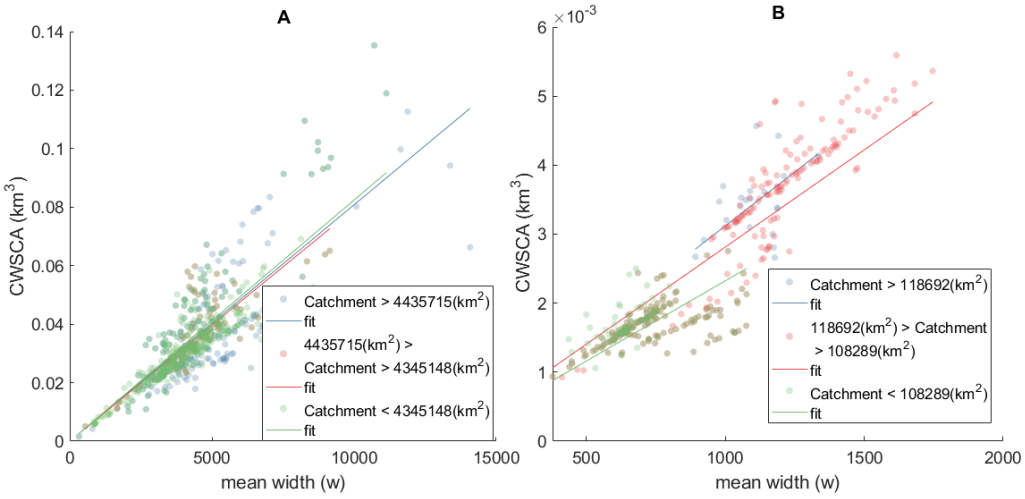

Figure 4. VCWSCA and mean width plots for the Amazon (A) and Uruguay (B) basins. Data is plotted by drainage area and fit with a least squares regression line per catchment regime. Data is grouped by large increases in in flow accumulation to avoid comparison across large tributaries. We then re-assimilated any divisions that did not achieve a change in basin drainage area>10 %.

Table 1.

Table 1 Percentage of GRACE TWS measure in main-stem CWS

River	% GRACE TWS	Basin drainage area (km^2)	CWS measured area (km^2)	GRWL inundated area (km^2)	CWS/ Width slope change with drainage area
Amazon	2.50	5,888,268	12,702	60,673	No
Amur	5.69	2,101,598	3,808	10,194	Yes
Ayeyarwada	5.29	385,438	1,449	3,199	No
Columbia	0.21	712,035	634	4,543	No
Congo	2.19	3,689,187	8,362	18,813	Yes
Ganges-Brahmaputra	3.02	1,792,035	5,293	15,160	No
Indus	2.20	864,062	935	4,330	-
Kolyma	2.43	657,254	1,928	5,150	-
Lena	0.51	2,467,695	9,507	20,836	-
Mackenzie	2.57	1,805,884	2,559	14,749	-
Mekong	2.89	773,231	2,244	18,197	Yes
Mississippi	1.69	3,244,506	2,709	17,002	Yes
Niger	0.45	2,115,246	642	7,019	-

Ob	1.71	2,929,051	4,757	15,176	-
Orinoco	4.96	937,352	2,899	7,537	No
Parana	1.12	2,639,954	6,096	20,843	Yes
SaoFrancisco	0.30	634,842	1,132	4,088	Yes
StLawrence	1.15	1,055,756	1,531	6,606	-
Tocantins	0.41	769,445	2,000	6,914	-
Uruguay	13.81	265,786	1,872	2,183	Yes
Volga	3.24	1,410,756	4,787	17,857	-
Yangtze	7.62	1,908,837	4,460	15,550	Yes
Yenisei	2.50	2,518,211	4,305	23,558	-
Yukon	1.42	1,373,188	2,067	6,687	-
Zambezi	0.05	1,373,188	504	7,186	Yes

487
488